IEEE Access
Multidisciplinary ⋮ Rapid Review ⋮ Open Access Journal

Received May 17, 2022, accepted June 3, 2022, date of publication June 13, 2022, date of current version June 20, 2022.

Digital Object Identifier 10.1109/ACCESS.2022.3182707

3D-Printed Broadband Power Divider Based on Helical-Microstrip Transmission Line Segments

JOSEP MARIA LOPEZ-VILLEGAS, (Senior Member, IEEE), NEUS VIDAL, AND ARNAU SALAS BARENYS

Department of Electronic and Biomedical Engineering, University of Barcelona (UB), 08028 Barcelona, Spain

Corresponding author: Josep Maria Lopez-Villegas (j.m.lopez_villegas@ub.edu)

This work was supported by the Spanish State Secretariat for Research, Development, and Innovation under Project TEC2017-83524-R.

ABSTRACT This paper presents the design and electromagnetic characterization of a 3D-printed 2-way broadband power divider intended to work in the RF band from several hundred MHz up to a few GHz. The design of the power divider is based on the use of helical-microstrip transmission line segments. Two different topologies of tapered helical-microstrip segments are considered prior to deciding on the final design of the power divider. The characteristic impedance profiles of both topologies are analyzed by means of electromagnetic simulation using the finite element method. After checking the performance of the segments in comparison with an ideal exponential profile, we propose an optimized design for the tapered impedance transformer. Two such optimized transformers are connected to configure the power divider as a compact 3-port device. We then fabricate and test a demonstrator prototype of this proposed broadband power divider design. Our experimental results show a good agreement with the performance predicted by electromagnetic simulations. These results demonstrate the potential of helical-microstrip technology to reduce the length of the transmission line segments required to implement such a power divider. A compaction factor of 4-5 was achieved, compared to an ideal design operating in the same frequency range.

INDEX TERMS 3D printing, broadband impedance transformer, broadband power divider, copper electroplating, helical-microstrip transmission lines, tapered transformer.

I. INTRODUCTION

Transmission line (TL) segments are building blocks used in a variety of microwave and RF components and circuits such as delay lines, filters, impedance transformers and couplers or power dividers/combiners, among others. The behavior of these components and circuits over a range of frequencies ultimately depends on the electromagnetic (EM) parameters of the TL segments, that is, their characteristic impedance and electrical length. Short segments (i.e., in the cm range) are required to implement the aforementioned components and circuits at microwave frequencies. Conversely, in the low band of the RF spectrum, the design of components and circuits based on TLs requires longer segments (i.e., tens of centimeters or more). Consequently, compaction of the TL segments is required to obtain practical designs for operation at low RFs.

In planar technologies meandering is the most common procedure adopted to compact TL segments. However, each bend in the meander line introduces a discontinuity that can affect propagation along the signal path. Current crowding in these discontinuities can become an important source of losses as the frequency increases. One way to avoid these discontinuities, while maintaining compaction, is to renounce planarity by using helical TLs. A helical TL is a coaxial line where one of the conductors is replaced by a helical spiral. If the cross-section of the spiral is a rectangle, then the geometry corresponds to a helical-microstrip TL. Apart from the phase factor, the current distribution does not change along the line, thus current crowding effects are avoided. In-depth analysis of the EM behavior of helical TLs can be found in [1] and [2]. Determination of the characteristic impedance and phase velocity in quasi-TEM propagation mode of a shielded helical TL width a round cross section can be found in [3]. As an example of their application, in [4] and [5] helical TLs are used to increase the pulse duration in pulsed power generation. More recently, EM modeling of 3D-printed helical-microstrip TL segments has been reported in [6]. Semi-empirical formulae for the characteristic impedance and the electrical length of such lines have been derived,

The associate editor coordinating the review of this manuscript and approving it for publication was Kai-Da Xu.

considering dependences on geometrical parameters as well as on the EM properties of the materials used. Compaction factors (specified as the electrical to physical length ratio) as high as 5 have been achieved without any appreciable effects on the characteristic impedance or group velocity of the line. This allows TL segments to be used in the design of components and circuits intended to operate in the low band of the RF spectrum.

In [7] Lopez-Villegas *et al.* study the use of helical-microstrip TL segments to implement broadband impedance transformers. They present preliminary results of the EM behavior of tapered helical-microstrip TL segments acting as broadband impedance transformers in the RF band from several hundred MHz up to a few GHz. Here, in this work, we now present extended analysis, considering this type of structure in more detail. We pay special attention to the control of the profile of the characteristic impedance along the segment in order to optimize performance. As a result, new strategies to obtain optimized tapered TL segments are proposed. Finally, as a demonstration of the potential of the helical-microstrip technology, and of the new optimized tapered TL segments, a prototype of a compact broadband 2-way power divider is presented.

The rest of the paper is organized as follows: In Section II, the profile of the characteristic impedance along tapered helical-microstrip TL segments is studied in detail as a function of their geometry. As a result of this study, a procedure to control the characteristic impedance profile is proposed and applied to find the optimum design of tapered impedance transformers. Then, in Section III, two optimized transformers are combined to implement a compact broadband 2-way power divider intended to work in the frequency range from 400 MHz to 2 GHz. Details of the fabrication process of the power divider, as well as the results of its EM characterization, are also discussed in this section. Finally, Section IV is devoted to present our conclusions and considering future directions and trends.

II. CHARACTERISTIC IMPEDANCE PROFILE OF TAPERED HELICAL-MICROSTRIP SEGMENTS

A. TAPERED LINES IN HELICAL-MICROSTRIP TECHNOLOGY

The simplest way to implement a tapered TL in standard microstrip technology is to vary the width of the metal strip along the line, according to a predefined profile. In an initial approach, a direct relationship is assumed between the width profile and the characteristic impedance profile along the line. For a given profile, different techniques have been proposed to analyze the EM behavior of tapered TLs [8]. Optimized profiles that minimize return losses have been proposed (see, e.g., [9] and [10]). However, linear [11] or exponential (e.g. [12] and [13]) profiles are also widely used, due to their simplified designs. Whatever the case, the objective of the strip width profile is to smoothly modify the characteristic impedance along the line to match the impedances connected

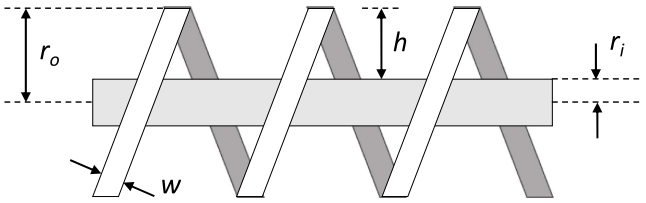

FIGURE 1. Schematic view of a helical-microstrip TL segment. The main geometrical parameters are the strip width w, the inner and outer radii, r_i, and r_o, respectively, and thickness $h = r_o - r_i$.

at both ends of the TL segment (i.e., Zo and Zl). In this configuration, the tapered line behaves like a high-pass filter. The cutoff frequency of such a filter, and also the ripple in the filter pass band, depend on the electrical length of the segment used to implement the tapered line: the longer the segment, the lower the filter cutoff frequency and the smaller the ripple in the filter passband. Consequently, electrically long tapered segments are required to increase bandwidth and reduce return losses.

It is in this context that the use of helical-microstrip technology reveals its potential as an alternative to standard microstrip technology. Due to their intrinsic 3D nature the electrical length of helical-microstrip TL segments is several times longer than their physical length. This feature is a great advantage of this technology when it comes to implementing compact tapered lines.

To understand how tapered lines can be implemented using helical-microstrip technology, let us consider the segment shown in Fig. 1. The view corresponds to a standard helical-microstrip TL segment. The inner conductor, which acts as a ground reference, is cylindrical in shape; the outer conductor is a helical-microstrip spiral. From [6], the characteristic impedance, Z_o, of the line is approximately given by:

$$Z_o = \frac{120\pi}{\sqrt{\varepsilon_{eff}}} \frac{h_{eff}}{w_{eff}} \tag{1}$$

where the effective substrate thickness, h_{eff}, is defined as:

$$h_{eff} = r_o ln\left(\frac{r_o}{r_i}\right) \tag{2}$$

It goes without saying that $h_{eff} \approx h = (r_o - r_i)$ if $r_o \approx r_i$.

In (1), the effective strip width, w_{eff}, is equal to the actual width, w, plus a correction term that accounts for the fringing effects. Except in the case of very narrow strips, we can assume, in an initial approach that $w_{eff} \approx w$. Finally, the effective permittivity, ε_{eff}, is an average for a medium consisting of the dielectric material that exists between the central conductor and the helical spiral and the surrounding air. Under these assumptions, expression (1) can be rewritten as:

$$Z_o = \frac{120\pi}{\sqrt{\varepsilon_{eff}}} \frac{h}{w} \tag{3}$$

According to (1), (2) and (3), the characteristic impedance, Z_o, can be profiled by varying either the thickness, h_{eff} (i.e., r_o and/or r_i), the width, w_{eff} (i.e., strip width, w), or both simultaneously.

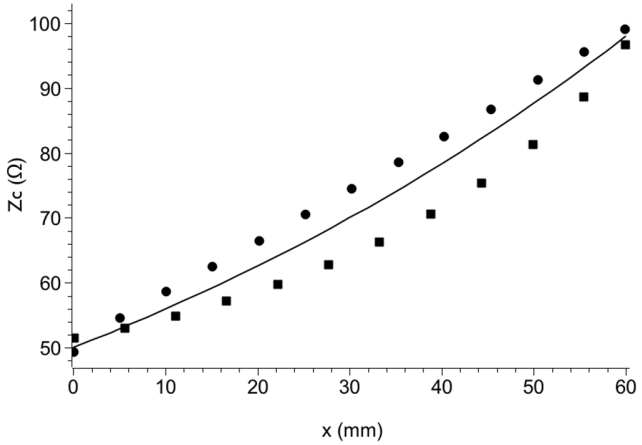

FIGURE 2. Profiles of the characteristic impedance of tapered helical-microstrip TL segments: squares correspond to the variable width case, and circles to the conical inner conductor case. The continuous line corresponds to the profile of an ideal exponential tapered TL segment.

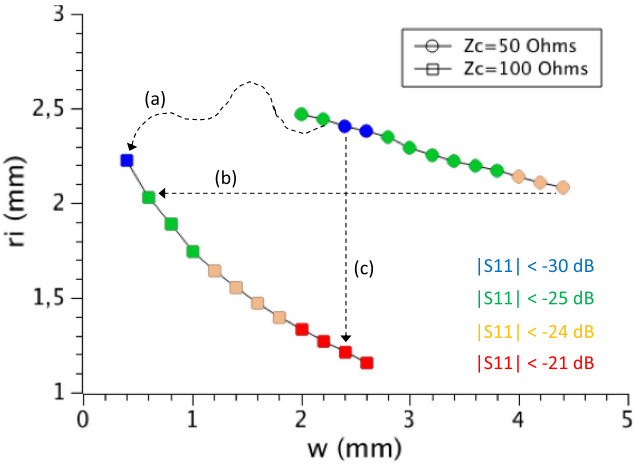

FIGURE 3. Plot of the constant characteristic impedance curves in the plane (w, r_i). Circles correspond to standard helical-microstrip segments with a 50Ω of characteristic impedance and squares to those with 100Ω. The different colors indicate maximum return losses across the entire frequency band of interest for a given segment. Different trajectories corresponding to actual implementations of impedance transformers are labeled as (a), (b) and (c).

In the previous work [6], two topologies of tapered helical-microstrip segments were considered to implement broadband impedance transformers. The first consisted of a TL segment with a variable strip width and a cylindrical inner conductor. The second consisted of a TL segment with a constant strip width and a conical inner conductor. In the first case, the width, w, was varied linearly along the TL segment. In the second case, the geometrical parameter that varied linearly along the TL segment was the inner radius, r_i. In both cases, the starting and ending values of the geometrical parameters were adjusted to match the impedance values of 50 Ω, at one end, and 100 Ω at the opposite end of the segment. These TL segments were successfully used to implement broadband impedance transformers, but the question that still arises is: Which characteristic impedance profile corresponds to a given profile of strip width or a given profile of the inner conductor? To answer this question, we selected several locations along each of the tapered segments. For each location the corresponding geometrical parameters, w, and r_i, were recorded and used to implement a CAD model of a uniform helical-microstrip TL segment with the same length as the original tapered segments (i.e., 60 mm). We used the FEM solver included in the EMPro design environment from Keysight Technologies Inc. to obtain S parameters as a function of frequency. Standard S parameter simulation using 50 Ω coaxial ports was carried out in the frequency range from 1 MHz to 2 GHz. Then, the characteristic impedance used as a reference for S parameters determination was tuned to minimize the return losses across the entire frequency range. Finally, this optimum value was assigned as the characteristic impedance of the uniform segments and also to the corresponding location along the tapered segment. Fig. 2 shows the characteristic impedance profiles obtained in this way for both topologies of tapered segment. For comparison purposes, the impedance profile corresponding to an optimum exponential transformer is also shown in the figure.

We can observe in the figure that the impedance profile corresponding to the variable width TL segment underestimates the characteristic impedance, compared to the exponential profile. Conversely, the impedance profile corresponding to the variable inner conductor TL segment overestimates the characteristic impedance. Accordingly, twe can expect that the right combination of strip width profile and inner conductor profile would lead to an optimum exponential or quasi-exponential profile of the characteristic impedance.

B. OPTIMIZING THE CHARACTERISTIC IMPEDANCE PROFILE

Before finding a combination of linear profiles that leads to the desired profile of the characteristic impedance, let us consider the "map" shown in Fig. 3. In this figure there are two curves that connect pairs of values (w, r_i) that correspond to helical-microstrip TL segments with characteristic impedances of 50 Ω and 100 Ω, respectively. For all the segments, the intermetal dielectric is a photopolymer used in material-jetting 3D printing. The EM parameters of the material were measured in the frequency band of interest using the rectangular cavity method and the coaxial waveguide method [14]. The results show a dielectric constant, $\varepsilon_r = 2.8 \pm 0.1$, and a loss tangent, $\tan\delta = 0.02 \pm 0.005$. In all the cases the number of turns of the helical spiral is: N=10, the length of the segment is: L=60 mm; and the outer radius is: $r_o = 3$ mm (i.e., the helical spiral radius).

The different colors of the curves correspond to the maximum values of the return losses across the entire frequency range of interest for a given segment. As a rule of thumb, the best values are obtained when r_i approaches r_o (i.e., $h_{eff} \approx h$).

Any trajectory starting on one curve and ending on the other, such as that labeled (a), corresponds to a functional impedance transformer. The trajectory is defined by two

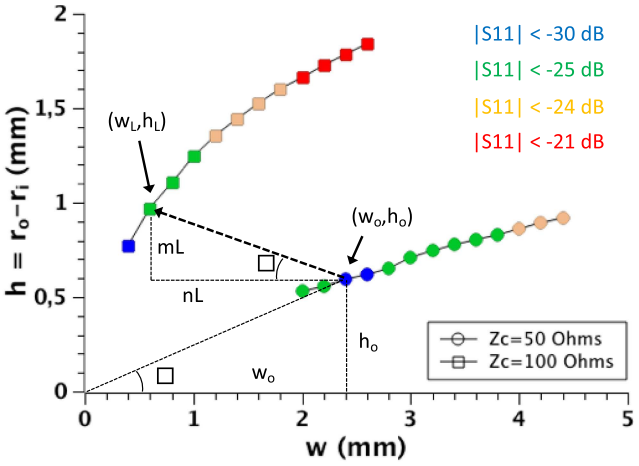

FIGURE 4. Plot of the constant characteristic impedance curves in the plane (*w*, *h*). Circles correspond to standard helical-microstrip segments with a 50 Ω characteristic impedance and squares to those with 100 Ω. The different colors indicate maximum return losses across the entire frequency band of interest for a given segment. The thick dashed line identifies one of the optimal trajectories that leads to an exponential profile of the characteristic impedance along the TL segment.

parametric functions: $w = f(x)$ and $r_i = g(x)$, where x identifies the location along the segment. The location, $x = 0$ mm, corresponds to the starting point on the 50 Ω curve, and the location, $x = L = 60$ mm, corresponds to the end point on the 100 Ω curve. Two additional trajectories are shown in the figure, labeled (b) and (c). In the case of trajectory (b), r_i is constant and w is a linear function of x. This is the case of the variable-strip-width transformer considered in previous work [7]. In turn, trajectory (c) corresponds to a constant width w, and a linear dependence of r_i on x. This is the case of the transformer with a variable inner conductor also considered in that previous work.

At this point, we can interpret the combination of the linear profiles of w and r_i as a straight trajectory connecting both curves with a certain slope. Finding the right combination to obtain the optimum exponential profile of the characteristic impedance is then reduced to finding the right slope. To do this, let us consider expression (3). Introducing linear dependences in r_i (i.e., in h) and w, we can rewrite this expression as:

$$\approx Z_c \frac{120\pi}{\sqrt{\varepsilon_{eff}}} \frac{h_o + mx}{w_o - nx} \tag{4}$$

where Zc is the characteristic impedance at location x, while h_o and w_o are the radius difference and the strip width at $x = 0$ (i.e., the 50 Ω side of the TL segment), respectively. Finally, m and n are the parameters that define the linear profiles in h and w, respectively. In expression (4) we consider that a decrease in r_i is equivalent to an increase in h. Taking the natural logarithm of both sides of the equation we obtain:

$$ln\,(Z_c) \approx ln\left(\frac{120\pi}{\sqrt{\varepsilon_{eff}}}\right) + ln\left(\frac{h_o + mx}{w_o - nx}\right) \tag{5}$$

Finally, differentiating with respect to x we have:

$$\frac{d}{dx}\,(ln\,(Z_c)) \approx \frac{mw_o + nh_o}{h_o w_o + (mw_o - nh_o)\,x - mnx^2} \tag{6}$$

If we want the profile of the characteristic impedance, Zc, to be exponential, then the derivative of its natural logarithm must be a constant, regardless of the value of x. According to (6) this requirement introduces two restrictions on the right-hand side of the equation. The first is:

$$mw_o \approx nh_o \tag{7}$$

so that the linear term in x in the denominator is reduced to zero. The second implies that the quadratic term in x in the denominator must be negligible, regardless of the value of x. The maximum contribution of the quadratic term corresponds to the case $x = L$. Accordingly, this term could be neglected if $h_o > mL$ and $w_o > nL$ (i.e., we have smooth profiles).

After all these considerations, we are in a position to determine the slope of the trajectory in the (*w*,*h*) plane that leads to the optimal exponential profile of the characteristic impedance. The parametric functions that describe the trajectory are the linear dependences of h and w, and the slope of the trajectory is given by:

$$s = -\frac{m}{n} \tag{8}$$

Finally, by substituting (7) into (8) the optimum slope can be written as:

$$s_{opt} \approx -\frac{h_o}{w_o} \tag{9}$$

In practice, the procedure for obtaining the optimal exponential profile of characteristic impedance consists of three steps: first a pair of (w_o, h_o) values corresponding to the starting point on the 50 Ω curve is selected. Then, a straight line is drawn passing through this starting point, and with a slope given by (9). At the intersect with the 100 Ω curve the end point (w_L, h_L) is determined. Finally, the linear parameters, m and n are obtained from the expressions:

$$m = \frac{h_L - h_o}{L} \tag{10}$$

and

$$n = \frac{w_o - w_L}{L} \tag{11}$$

The whole process is depicted in Fig. 4. In this figure the curves corresponding to a 50 Ω and a 100 Ω of characteristic impedance are plotted in the (*w*,*h*) plane. The optimum trajectory is indicated as a straight line connecting the starting point at the (w_o, h_o) on the 50 Ω curve to the end point (w_L, h_L) on the 100 Ω curve. The optimal slope criterion previously discussed is specified by the angle, α.

Two optimal trajectories were considered in this work. The first is that shown in Fig.4, from now on called trajectory T1. The starting point at the 50 Ω end of the tapered helical-microstrip TL segment corresponds to: $w_o = 2.4$ mm, and $h_o = 0.6$ mm (i.e., $r_i = 2.4$ mm). The end point at the 100 Ω

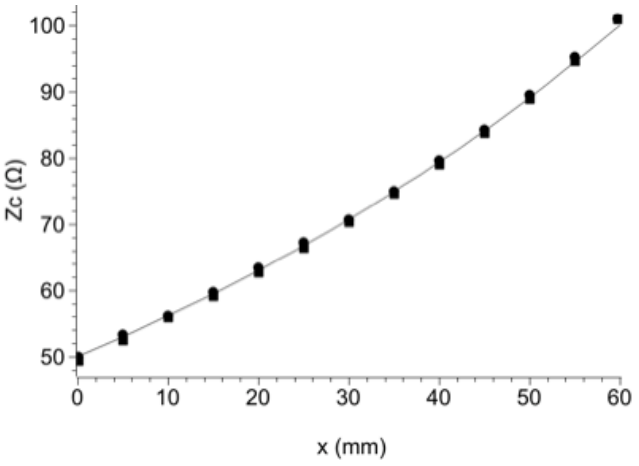

FIGURE 5. Profiles of the characteristic impedance of the helical-microstrip transformers corresponding to optimal trajectories T1 (circles) and T2 (squares). The continuous line corresponds to the profile of an ideal exponential tapered transformer.

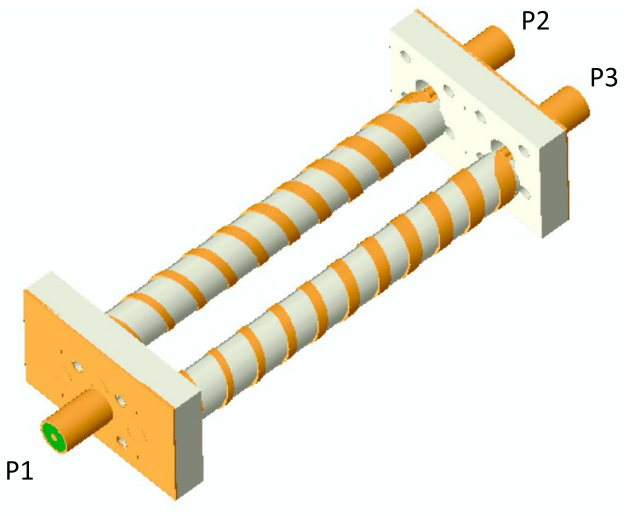

FIGURE 6. CAD model of the compact broadband 2-way power divider. The component consists of two optimized broadband impedance transformers and three SMA connectors. The nominal impedance at all ports is 50 Ω.

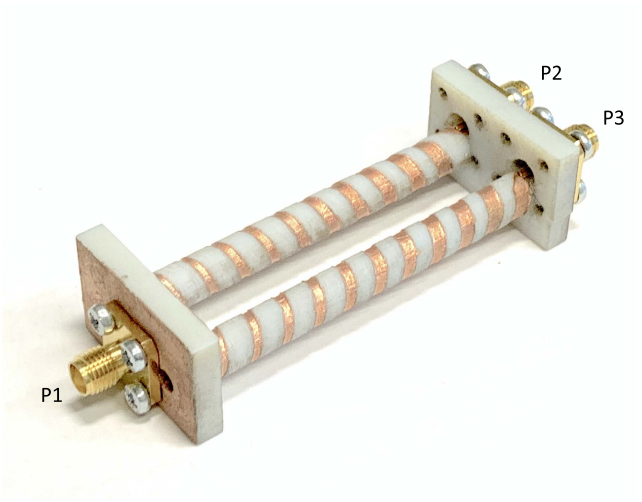

FIGURE 7. View of the compact broadband 2-way power divider prototype. The length is 90.6 mm (73 mm without SMA connectors), the width is 30 mm, and the height is 19 mm.

end of the tapered segment corresponds to: $w_L = 0.65$ mm, and $h_L = 0.95$ mm (i.e., $r_i = 2.05$ mm). The second trajectory, T2, corresponds to the starting and end points: $w_o = 2.8$ mm, $h_o = 0.65$ mm (i.e., $r_i = 2.35$ mm), and $w_L = 0.8$ mm, $h_L = 1.15$ mm (i.e., $r_i = 1.85$ mm), respectively. In both cases the length of the segments is: $L = 60$ mm, and the outer radius is: $r_o = 3$ mm. For each trajectory, the profile of the characteristic impedance was evaluated as previously explained; Fig. 5 shows the results. It is worth highlighting the good agreement between the profile obtained from FEM simulations and the ideal exponential profile. The maximum relative error is 1.3%, which verifies the accuracy of the proposed method. Finally, given that (4) can also identify the characteristic impedance of a standard microstrip TL, it follows that the proposed method could also be applied to that technology, provided that the thickness of the substrate can be modified linearly.

III. COMPACT BROADBAND 2-WAY POWER DIVIDER

As an additional demonstration of the potential of helical-microstrip technology, two optimized broadband impedance transformers were connected to configure a compact 3-port device. Fig. 6 shows a CAD model of the resulting assembly. The optimized transformers correspond to trajectory T2. The reason for choosing T2 rather than T1 is that the strip of the helical spiral is wider than for T1, which reduces the impact of printing tolerances, without occasioning a significant degradation of the impedance match.

The nominal impedance for all ports (i.e., P1, P2 and P3) is 50 Ω. Ports P2 and P3 are connected to the 50 Ω end of the impedance transformers. Accordingly, the impedance at the end of the segments is 100 Ω. Then, the segments terminations are connected in parallel at port P1, leading to a load impedance of 50 Ω. As a result, return losses are nominally zero at port P1 and the incident power is equally distributed between ports P2 and P3. As we will discuss latter, it should be noted that ports P2 and P3 are not matched or isolated, as they would be in a Wilkinson power divider/combiner. Our design is a broadband power divider. Therefore, it focusses on broadband power transfer from port 1 to ports 2 and 3, minimizing returns losses as long as ports 2 and 3 are loaded with the characteristic impedance. To fabricate a prototype of this compact broadband 2-way power divider we used a material jetting (Polyject) 3D printer, model Objet260 Connex 1 from Stratasys Ltd, in combination with copper plating. Depending on the geometry of the areas to be metallized, electroless copper plating, copper electroplating or a combination of both techniques was used. This procedure has previously been used to fabricate 3D conical inductors and capacitors (see [15] and [16]). The process started with the CAD model shown in Fig. 6. All the metallic areas of the model, including the helical spirals, were intentionally buried up to 50% of their thickness within the dielectric material. Then, the first step

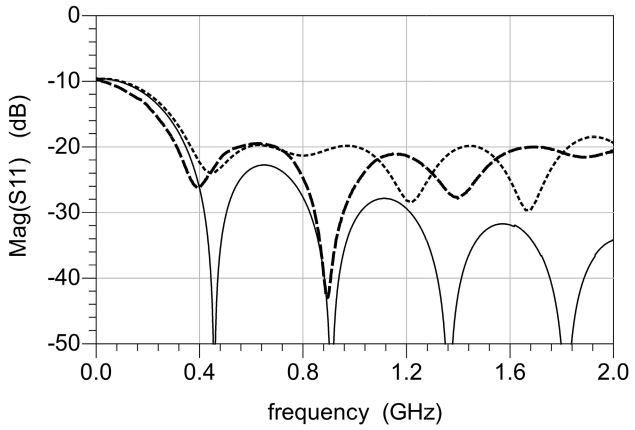

FIGURE 8. Magnitude of the S11 parameter of the compact broadband power divider. The dashed line corresponds to the measured response of the prototype shown in Fig. 7. The dotted line corresponds to the FEM simulation results of the CAD model reproduced in Fig. 6, and the thin continuous line corresponds to the response of an ideal exponential broadband power divider.

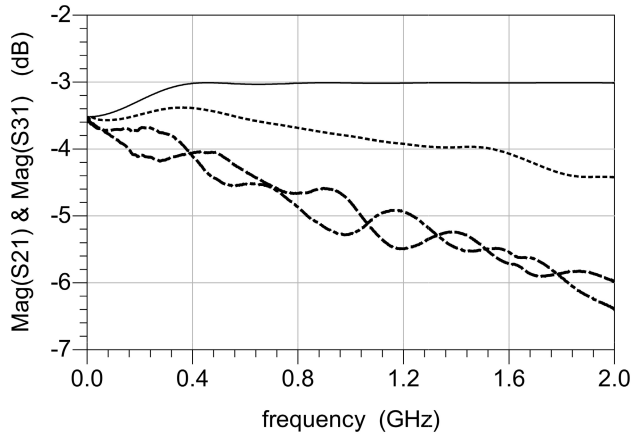

FIGURE 9. Magnitudes of the S22 and S33 parameters of the compact broadband power divider. The dashed line (S22) and dot-dashed line (S33) correspond to the measured response of the prototype shown in Fig. 7. The dotted line corresponds to the FEM simulation results of the CAD model reproduced in Fig. 6, and the thin continuous line corresponds to the response of an ideal exponential broadband power divider.

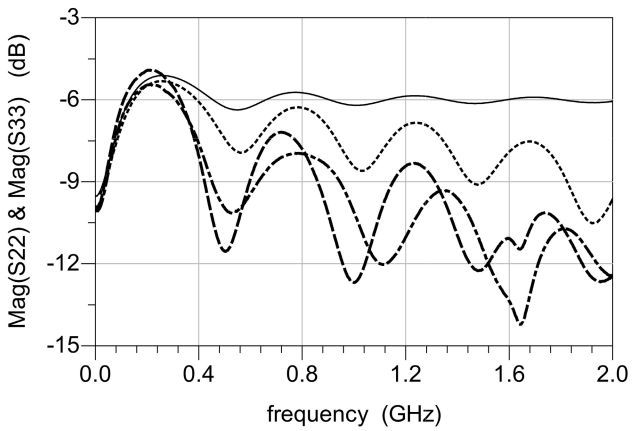

FIGURE 10. Magnitudes of the S21 and S31 parameters of the compact broadband power divider. The dashed line (S21) and dot-dashed line (S31) correspond to the measured response of the prototype shown in Fig. 7. The dotted line corresponds to the FEM simulation results of the CAD model reproduced in Fig. 6, and the thin continuous line corresponds to the response of an ideal exponential broadband power divider.

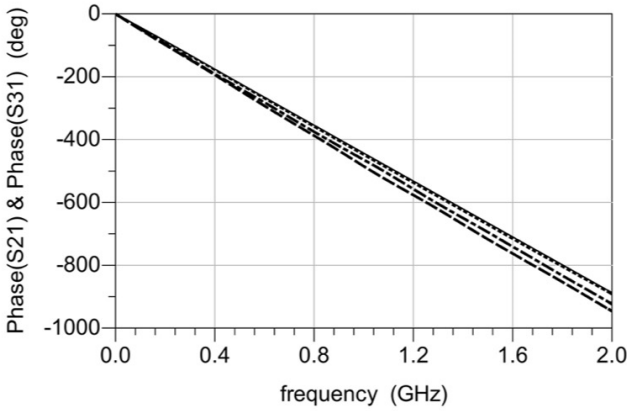

FIGURE 11. Phases of the S21 and S31 parameters of the compact broadband power divider. The dashed line (S21) and dot-dashed line (S31) correspond to the measured response of the prototype shown in Fig. 7. The dotted line corresponds to the FEM simulation results of the CAD model reproduced in Fig. 6, and the thin continuous line corresponds to the response of an ideal exponential broadband power divider.

consisted of using Boolean operators to subtract the metallic areas from the dielectric base. This led to a part consisting of two cylinders, each with an internal hollow in the form of a cone and a helical trench of variable width on each external surface. Pads to attach the SMA connectors were added at both ends. The resulting part was 3D printed and then coated using a silver ink spray. The function of the silver ink was to act as a seed for metal growth. Consequently, it was removed from unwanted areas by polishing. Finally, a copper layer was grown where the silver ink remained (i.e., the helical trenches, the inner hollows, and the pad surfaces). Fig. 7 offers a view of the final prototype after metallization and assembly of the SMA connectors. The dimensions of this prototype, including connectors, were: 90.6mm × 30mm × 18.8mm.

The S parameters of the power divider prototype were measured, in the range from 1 MHz to 2 GHz, using an E5071C Vector Network Analyzer (VNA) from Keysight Technologies, Inc. Prior to the measurements, the VNA was calibrated in the frequency range of interest using an electronic calibration module N4431-60003, also from Keysight Technologies Inc. Fig. 8 shows the magnitude in dB of the S11 parameter of the power divider prototype as a function of frequency. For comparison purposes, FEM simulation results for the CAD model in Fig. 6, and the response of an ideal exponential divider are also plotted in the figure. The matching band starts at 312 MHz for the manufactured prototype, and at 360 MHz for the CAD model, and continues up to 2 GHz in both cases. Concerning the upper limit of return losses in the matching band, it is about −20 dB, whether measured or simulated. It is worth noting that this broadband behavior far exceeds the matching bandwidth of a Wilkinson device acting as a power divider [17]. In both cases, the return losses degrade with respect to the ideal exponential divider as the frequency increases. In both cases, the observed

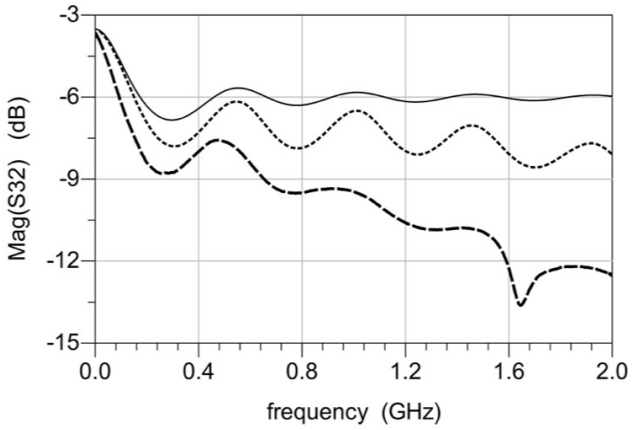

FIGURE 12. Magnitude of the S32 parameter of the compact broadband power divider. The dashed line corresponds to the measured response of the prototype shown in Fig. 7. The dotted line corresponds to the FEM simulation results of the CAD model reproduced in Fig. 6, and the thin continuous line corresponds to the response of an ideal exponential broadband power divider.

discrepancies could be related to tolerances in the printing process (i.e., 60 μm in the XY plane and 20 μm in the Z direction), and dispersion due to the frequency dependence of the dielectric constant of the printing material (i.e., from 2.9 at 1MHz to 2.7 at 2 GHz). It is also worth noting that the ideal exponential divider that best fits the experimental and simulation results is 348.8 mm long (including SMA connectors and considering air as the dielectric). This corresponds to a compaction factor of 3.85 (4.6 without the SMA connectors). Fig. 9 shows the magnitude in dB of the S22 and S33 parameters as a function of frequency. As expected, ports 2 and 3 are not matched. Data for the ideal power divider indicate that return losses are about 6 dB in the operating frequency band. Simulation and measurement data show an increase in return losses that could also be related to printing tolerances and dispersion of the dielectric constant.

Fig. 10 shows the magnitude in dB of the transmission parameters. The increase of attenuation with respect to the ideal exponential divider can be as much as 1.5 dB for the CAD model using FEM simulations, and up to 3 dB for the prototype measurements, both determined at the upper limit of the frequency band (i.e., 2 GHz). In this case the discrepancies are due to the conductivity of the metal parts. For the FEM simulation the conductivity of bulk copper is considered (i.e., 5.8×10^6 S/m). In contrast, for the measurements using the prototype the conductivity of the metal could be affected by residual silver ink on the dielectric-facing surface or by the structure of the electroplated copper (i.e., grain size, impurities in the grain boundaries, voids, etc.). However, analysis of these phenomena is beyond the scope of this work. These phenomena may also explain the unbalance between the measured magnitudes of the S21 and S31 parameters; although it is always less than 0.7 dB across the entire frequency band from 1 MHz to 2 GHz. Fig. 11 shows the phase, in degrees, of the transmission parameters. The data corresponding to the ideal divider and the CAD model

TABLE 1. Main characteristics of the proposed broadband power divider.

Matching |Bandwidth |S11| @(-20dB)	Matching |S22| & |S33|	Isolation |S32|	Insertion losses |S21| & |S31|	Mag unbalance |S21| vs |S31|	Phase unbalance S21 vs S31
(0.35-2) GHz	< -6 dB	< -6dB	≈1dB + 1dB every 0.8 GHz	< 0.7 dB	1 degree every 0.1 GHz

reproduced in Fig. 6 show a linear dependence of phase on frequency. There are only minor differences between the two datasets. Our measured results show a deviation from the linear behavior which could be explained by dispersion of the dielectric constant. Moreover, there is also an unbalance between the phases at ports 2 and 3. The phase difference increases at a rate of about 1 degree every 100 MHz. This behavior can be explained by the previously mentioned inhomogeneities in the metallization process.

Fig. 12 shows the magnitude of the S23 parameter in dB. As expected, ports 2 and 3 are not isolated. Data for the ideal power divider indicate that ports isolation is only about 6 dB in the operating frequency band. Simulation and measurement data show better isolation which could be related to transmission losses as well as printing tolerances and dispersion of the dielectric constant.

As a final summary, table 1 shows the main features of the proposed broadband power divider.

IV. CONCLUSION

In this work we present the design, manufacture, and EM characterization of a compact broadband 2-way power divider intended to work in the RF band from several hundred MHz up to a few GHz. The design is based on the use of helical-microstrip technology. The EM behavior of impedance transformers implemented as tapered helical-microstrip TL segments is studied in detail. Two different geometries of tapered TL segments are considered. The first consists of linearly varying the width of the helical spiral to match the impedances connected at both ends of the segment. The second uses an inner tapered ground conductor instead of an inner ground cylinder. After demonstrating the potential of helical-microstrip technology to implement broadband impedance transformers, a study of the characteristic impedance profile along the segments is carried out. The correspondence between the impedance profile and the strip width and inner-conductor profiles is established. From comparisons with the impedance profile of an ideal exponential transformer, a method to optimize the tapered helical-microstrip TL segments is proposed. We devise a systematic procedure to simultaneously modify the spiral strip width and the radius of the inner conductor that leads to a quasi-exponential profile of the characteristic impedance.

As a final demonstration, we implemented a compact 2-way broadband power divider using a pair of optimized tapered helical-microstrip TL segments. A combination of material-jetting 3D printing and copper plating is used to manufacture the prototype. Experimental measurements agree with the simulation results and show that the operating band of the divider ranges from 312 MHz up to 2 GHz with an upper limit of return losses of about -20 dB and insertion losses below 3 dB across the entire frequency band of interest.

Further work is currently underway to expand the use of helical-microstrip technology to other applications in the RF band.

REFERENCES

[1] V. Fowler, "Analysis of helical transmission lines by means of the complete circuit equations," *Trans. IRE Prof. Group Antennas Propag.*, vol. 2, no. 4, pp. 132–143, Oct. 1954.
[2] W. Sichak, "Coaxial line with helical inner conductor," *Proc. IRE*, vol. 42, no. 8, pp. 1315–1319, Mar. 1955.
[3] H. S. Kirschbaum, "The characteristic impedance and phase velocity of a shielded helical transmission line," *Trans. Amer. Inst. Electr. Eng. I, Commun. Electron.*, vol. 78, no. 4, pp. 444–450, Sep. 1959, doi: 10.1109/TCE.1959.6372842.
[4] S. K. Sharma, P. Deb, A. Sharma, R. Shukla, T. Prabaharan, B. Adhikary, and A. Shyam, "Compact Helical pulse forming line for the generation of longer duration rectangular pulse," *Rev. Sci. Instrum.*, vol. 83, no. 6, 2012, Art. no. 066103, doi: 10.1063/1.4727869.
[5] E. L. Ruden, "Helical pulse-forming transmission line stack for compact pulsed power applications—Design and simulation," in *Proc. IEEE 21st Int. Conf. Pulsed Power (PPC)*, Jun. 2017, pp. 1–6.
[6] J. M. Lopez-Villegas, A. Salas, and N. Vidal, "Modeling of 3-D-printed helical-microstrip transmission lines for RF applications," *IEEE Trans. Microw. Theory Techn.*, vol. 67, no. 12, pp. 4914–4921, Dec. 2019.
[7] J. M. Lopez-Villegas, A. Salas, and N. Vidal, "3D-printed broadband impedance transformers using helical-microstrip transmission line segments," in *IEEE MTT-S Int. Microw. Symp. Dig.*, Los Angeles, CA, USA, Aug. 2020, pp. 892–895.
[8] M. H. Eghlidi, K. Mehrany, and B. Rashidian, "Analytical approach for analysis of nonuniform lossy/lossless transmission lines and tapered microstrips," *IEEE Trans. Microw. Theory Techn.*, vol. 54, no. 12, pp. 4122–4129, Dec. 2006, doi: 10.1109/TMTT.2006.885565.
[9] R. E. Collin, "The optimum tapered transmission line matching section," *Proc. IRE*, vol. 44, no. 4, pp. 539–548, Apr. 1956.
[10] R. W. Klopfenstein, "A transmission line taper of improved design," *Proc. IRE*, vol. 44, pp. 15–31, Jan. 1956.
[11] C. L. Edwards, M. L. Edwards, S. Cheng, R. K. Stilwell, and C. C. Davis, "A simplified analytic CAD model for linearly tapered microstrip lines including losses," *IEEE Trans. Microw. Theory Techn.*, vol. 52, no. 3, pp. 823–830, Mar. 2004, doi: 10.1109/TMTT.2004.823545.
[12] M. Kobayashi and N. Sawada, "Analysis and synthesis of tapered microstrip transmission lines," *IEEE Trans. Microw. Theory Techn.*, vol. 40, no. 8, pp. 1642–1646, Aug. 1992, doi: 10.1109/22.149542.
[13] C. Zheng and T. Li, "Development of an exponential tapered impedance transformer for UHF-PD sensor," in *Proc. 1st Int. Conf. Electr. Power Equip. Switching Technol.*, Xi'an, China, Oct. 2011, pp. 383–386.
[14] A. Salas-Barenys, N. Vidal, J. Sieiro, J. M. López-Villegas, B. Medina-Rodriguez, and F. M. Ramos, "Full-3D printed electronics process using stereolitography and electroless plating," in *Proc. 32nd Conf. Design Circuits Integr. Syst. (DCIS)*, Nov. 2017, pp. 1–4, doi: 10.1109/DCIS.2017.8311624.
[15] J. M. Lopez-Villegas, N. Vidal, J. Sieiro, A. Salas, B. Medina, and F. M. Ramos, "Study of 3-D printed conical inductors for broadband RF applications," *IEEE Trans. Microw. Theory Techn.*, vol. 66, no. 8, pp. 3597–3602, Aug. 2018.
[16] J. M. Lopez-Villegas, A. Salas, N. Vidal, and J. Sieiro, "3D-printed low-pass filter with conical inductors for broadband RF applications," in *Proc. 48th Eur. Microw. Conf. (EuMC)*, Madrid, Spain, Sep. 2018, pp. 292–295.
[17] D. M. Pozar, "Power dividers, directional couplers, and hybrids," in *Microwave Engineering*, 2nd ed. Reading, MA, USA: Addison Wesley, 1993, pp. 395–401.

JOSEP MARIA LOPEZ-VILLEGAS (Senior Member, IEEE) received the Ph.D. degree in physics from the University of Barcelona, Barcelona, Spain, in 1990. He is currently the Director of the Group of Excellence for Radio Frequency Components and Systems, University of Barcelona, where he is also a Full Professor with the Department of Electronic and Biomedical Engineering. His research interests include the design, optimization, and test of RF components; circuits and systems performed using silicon, multilayered technologies, such as multichip modules and low-temperature co-fired ceramics, and 3D printing; the use of 3D simulators for electromagnetic analysis of RF components, circuits and systems; the analysis of electromagnetic compatibility and electromagnetic interference problems; the interaction of electromagnetic energy with biological tissues; the modeling and optimization of integrated inductors and transformers for general RF applications; and the development of new homodyne transceiver architectures based on injection-locked oscillators.

NEUS VIDAL received the Ph.D. degree in physics from the University of Barcelona, Spain 1995. Currently she is a Full Professor with the University of Barcelona and a member with the Group of Excellence for Radio Frequency Components and Systems, University of Barcelona. Her current interests include electromagnetic analysis of RF components, circuits, and systems, and additive manufacturing techniques for the design and implementation of non-planar fully 3D printed devices.

ARNAU SALAS BARENYS received the B.E. degree in electronics engineering of telecommunication from the Universitat de Barcelona (UB), Spain, the M.S. degree in telecommunication engineering from the Universitat Autònoma de Barcelona (UAB), Spain, in 2017, and the Ph.D. degree from the University of Barcelona (UB), in 2021. His research interests include electronics design, radiofrequency and electromagnetic modeling, communication systems, 3D design, and 3D printing.